Journal of Structural Geology, Vol. 15, Nos 3–5, pp. 323 to 334, 1993
Printed in Great Britain

0191-8141/93 $06.00+0.00

The geometry of echelon fractures in rock: implications from laboratory and numerical experiments

ANDREW L. THOMAS

Department of Geology, Stanford University, Stanford, CA 94305, U.S.A.

and

DAVID D. POLLARD

Departments of Applied Earth Sciences and Geology, Stanford University, Stanford, CA 93405, U.S.A.

(*Received* 30 *December* 1991; *accepted in revised form* 28 *July* 1992)

Abstract—The traces of echelon joints, veins and dikes in rock range from curving to straight. Theoretical analyses using boundary element numerical methods have concluded that straight, open fractures imply a significant remote differential stress whereas curving traces imply a more nearly isotropic stress. We present a series of laboratory experiments which investigate the two-dimensional propagation paths of echelon fractures in PMMA plates as a function of the applied biaxial loading and the initial geometry of a simple fracture array. The experimental results support the theoretical conclusions and verify the accuracy of the numerical method.

At the grain scale, rock does not rigorously conform to the assumptions of isotropy, homogeneity and linear elasticity demanded by the numerical method. Nevertheless, results from crack path stability theory suggest that small-scale deviations of a fracture from the ideal path generally do not affect its large-scale behavior. Fracture paths which become kinked or curved by local heterogeneities are found to self-correct to a path governed by competition between the fracture tip and remote stress fields, provided the remote differential stress is non-zero. This enhances our confidence that the numerical method can be used to produce and explain realistic fracture geometries in rock.

An unexpected experimental result is the non-perpendicular intersection of fractures grown in the laboratory. Free surface boundary conditions require that the walls of an open fracture be free of shear stress. The principal stresses are therefore aligned with the crack wall, and we might consequently expect an approaching opening mode fracture either to intersect the free surface at a right angle or to turn away and follow an asymptotic, non-intersecting path. Experimental and numerical modeling, however, shows how the near-tip stresses generated by an approaching fracture dominate the local stress field and allow it to propagate along an oblique path very close to intersection with the adjacent free surface.

INTRODUCTION

OUR ability to infer paleostress conditions from the geometry of joints, veins and dikes has benefited greatly from advances in the field of fracture mechanics. Methods have been introduced to relate joint and dike orientation to principal stress trajectories (Odé 1957, Muller & Pollard 1977, Engelder & Geiser 1980), joint and dike dilation to driving stress magnitude (Pollard & Muller 1976, Delaney & Pollard 1981, Segall & Pollard 1983), joint kinking or curvature to remote differential stress (Olson & Pollard 1989, Cruikshank *et al.* 1991), and echelon vein and joint traces to shear deformation (Shainin 1950, Ramsay 1980), rotation of the remote stress field (Pollard *et al.* 1982), and mechanical fracture interaction (Olson & Pollard 1991).

Numerical methods are capable of explaining a wide range of fracture problems which lack simple analytic solutions. Using a boundary element numerical model, Olson & Pollard (1989) related the curvature of overlapping joint traces to the magnitude of the remote differential stress. They found that straight joints imply a significant remote differential stress whereas curving traces imply a more nearly isotropic remote stress. Here, we consider the same problem but adopt a laboratory experimental approach, investigating the two-dimensional propagation paths of echelon fractures in PMMA plates as a function of the applied biaxial loading and the initial geometry of a simple fracture array. Because the experimental boundary conditions and material properties are well known, they provide an excellent basis for evaluating the accuracy of the numerical method. We also present arguments based on crack path stability which suggest that grain-scale heterogeneities encountered in rock will not significantly alter the propagation paths from those predicted by the numerical model.

THEORETICAL BACKGROUND

If we assume a homogeneous, linear elastic, isotropic solid, linear elastic fracture mechanics can be used to compute the near-tip stresses and predict fracture behavior. Here, we consider a single layer or bed of rock subject to uniform remote stresses, σ_{ij}^{r}, where tension is positive and the shear stresses ($i \neq j$) are positive in the directions shown (Fig. 1a). The components of remote stress are related to the local stresses by

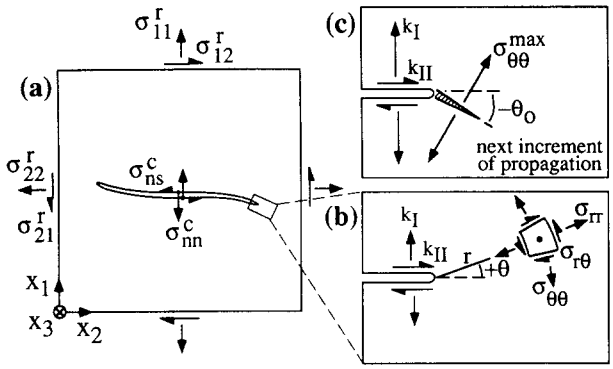

Fig. 1. (a) An isolated fracture is subject to remote stresses (σ^r_{11}, σ^r_{22}, σ^r_{12}) and surface tractions (σ^c_{nn}, σ^c_{ns}). All stresses are positive as drawn. Material properties, geometry and loading do not change with x_3, and plane strain conditions are assumed. (b) The magnitude of near-tip stresses (σ_{rr}, $\sigma_{\theta\theta}$, $\sigma_{r\theta}$) is proportional to the mode I (opening) and mode II (shearing) stress intensity factors, k_I and k_{II}. (c) Mixed mode I–II loading causes the propagating fracture to deviate from a straight path. The fracture grows in a radial direction from the crack tip and starts in the plane perpendicular to the direction of greatest tension, $\sigma^{max}_{\theta\theta}$.

$$\sigma^r_{ij} = \lim_{|x|\to\infty} \sigma_{ij}. \tag{1}$$

Material properties, loading conditions and geometry do not change with x_3. Since the u_3 component of displacement is assumed zero everywhere, the components u_1 and u_2 are functions only of the co-ordinates x_1 and x_2. Accelerations are sufficiently small so that inertial forces can be neglected relative to static forces. The analysis is therefore reduced to two-dimensional, elastostatic plane strain, and only the in-plane components of stress and displacement need to be considered.

A crack of negligible thickness penetrating the x_1–x_2 plane is subject to surface tractions σ^c_{ns} and σ^c_{nn} due to friction and/or internal fluid pressure. The tractions are considered positive when they act to the right of and in the same direction as the outward normal to the surface, respectively (Fig. 1a). In this paper, we assume the crack walls are open and separated by a fluid phase such as air or water, so $\sigma^c_{nn} = -p$ and $\sigma^c_{ns} = 0$, where p is the fluid pressure. If we restrict our attention to a small region near the fracture tip (Fig. 1b), we can idealize the fracture front as a straight line and the fracture surfaces as perfectly planar. Following the conventions of fracture mechanics (Irwin 1960, Lawn & Wilshaw 1975), the two possible directions of crack wall displacement discontinuity correspond to the two modes of in-plane fracture loading: opening (mode I) and sliding (mode II). Taking polar co-ordinates centered at the fracture tip, the near-tip stresses are approximated by (Erdogan & Sih 1963)

$$\sigma_{rr} \cong \frac{1}{(2\pi r)^{1/2}} \cos\frac{\theta}{2}\left\{k_I\left(1 + \sin^2\frac{\theta}{2}\right) + k_{II}\left(\frac{3}{2}\sin\theta - 2\tan\frac{\theta}{2}\right)\right\} \tag{2a}$$

$$\sigma_{\theta\theta} \cong \frac{1}{(2\pi r)^{1/2}} \cos\frac{\theta}{2}\left\{k_I \cos^2\frac{\theta}{2} - k_{II}\frac{3}{2}\sin\theta\right\} \tag{2b}$$

$$\sigma_{r\theta} \cong \frac{1}{2(2\pi r)^{1/2}} \cos\frac{\theta}{2}\left\{k_I \sin\theta + k_{II}(3\cos\theta - 1)\right\}, \tag{2c}$$

where k_I and k_{II} are the mode I and mode II stress intensity factors whose values depend on such factors as loading conditions, crack length and crack shape. In keeping with most of the fracture mechanics literature, we include a $\pi^{1/2}$ term in the denominator that Erdogan & Sih (1963) omit, so that our ks differ from theirs by a factor of $\pi^{1/2}$. For a straight crack of half-length, c, subject to uniform loading, Pollard & Segall (1987) show that equations (2a)–(2c) are accurate to within 15% of the exact solution over distances ranging from $r < 0.01c$ directly ahead of the crack tip ($\theta = 0°$) to $r < 0.15c$ along the crack surfaces ($\theta = \pm 180°$). Of course, the stress singularity predicted by equations (2a)–(2c) at the tip ($r = 0$) is not actually achieved in nature because inelastic deformation prevents the crack tip from being perfectly sharp. The linear elastic criteria for fracture propagation that we use here are valid if the region of inelastic deformation is small compared to the size of the near-tip field (i.e. $r \ll 0.15c$).

Classical elastic fracture mechanics states that an opening mode fracture will propagate dynamically when the mode I stress intensity factor, k_I, exceeds the fracture toughness of the material, k_{Ic}, and so long as loading remains pure mode I, the propagating fracture will follow a straight path (Lawn & Wilshaw 1975, Broberg 1987). Propagation by means of mode II shear separation ($k_{II} > k_{IIc}$) is difficult to attain, and laboratory experiments (Erdogan & Sih 1963, Ingraffea 1981, Petit & Barquins 1988) and theoretical arguments (Melin 1986, 1987) have demonstrated that even under pure mode II loading, mode I failure is usually strongly preferred. Apparently, mode II failure requires high confining pressure and frictional slip along closed crack walls. When an opening mode fracture is subject to mixed mode I–II loading, the net effect is a rotation of the most tensile principal stress to an angle which is no longer orthogonal to the fracture tip (Fig. 1c). In its next increment of propagation, the fracture tip attempts to reorient itself so that pure mode I loading is restored. Temporally continuous propagation under smoothly changing mixed mode I–II loading produces smoothly curving paths (Radon *et al.* 1977, Bergkvist & Guex 1979, Cotterell & Rice 1980), whereas a pronounced change in k_{II}/k_I while the fracture is not propagating produces a sharp kink in the path when propagation resumes (Erdogan & Sih 1963, Ingraffea 1981). The magnitude of the ratio k_{II}/k_I determines the magnitude of change in propagation angle, and the sign of k_{II}/k_I determines the direction (right-lateral shear yields right-curving paths and vice versa).

Fracture path curvature in a developing fracture set

An isolated fracture which propagates under uniform loading will assume a planar geometry perpendicular to the most tensile remote principal stress, σ^r_1. Setting the

x_2 axis parallel to the fracture plane gives $\sigma^r_{11} = \sigma^r_1$, $\sigma^r_{22} = \sigma^r_2$ and $\sigma^r_{12} = 0$. The stress intensity factors for this planar, isolated crack are given by (Lawn & Wilshaw 1975)

$$k_I = (\sigma^r_{11} - \sigma^c_{nn})(\pi c)^{1/2} = (\sigma^r_1 + p)(\pi c)^{1/2} \quad (3a)$$

$$k_{II} = \sigma^r_{12}(\pi c)^{1/2} = 0, \quad (3b)$$

where $2c$ is the crack length, $p = -\sigma^c_{nn}$ is the internal fluid pressure, and $(\sigma^r_1 + p)$ is called the fracture driving stress. Equations (3a) and (3b) state that propagation from a straight crack is independent of the crack-parallel component of remote stress σ^r_2. Cotterell & Rice (1980), however, have shown that the extension of a kinked or slightly curved crack is sensitive to the magnitudes of all components of the stress field. Specifically, a large crack-parallel remote differential stress, $\Delta\sigma^r = \sigma^r_1 - \sigma^r_2$, induces shear (mode II) stress across the tip of a kinked crack which would tend to turn it back toward a straight path (Fig. 2).

When fractures are not isolated, as in a developing set containing closely spaced members, adjacent fractures or fracture segments mechanically interact to produce non-uniform, mixed mode loading, and the resulting propagation paths can be significantly curved (Swain & Hagan 1978, Sempere & Macdonald 1986, Fleck 1991). Many naturally occurring fracture sets, however, display straight fracture traces, despite the close spacing and large overlap of their members (Segall & Pollard 1983, Cruikshank *et al.* 1991). Olson & Pollard (1989) employed boundary element modelling to demonstrate that a large crack-parallel remote differential stress inhibits the curvature of interacting as well as isolated fractures. Cruikshank *et al.* (1991) arrive at the same conclusion using Sumi *et al.*'s (1985) extension of the curved-crack analysis of Cotterell & Rice (1980) to include the effect of stress gradients arising from fracture interaction or nearby boundaries. They show that for a given fracture spacing, the paths of interacting, parallel fractures are sensitive to the remote stress-difference ratio,

$$R = (\sigma^r_1 - \sigma^r_2)/(\sigma^r_1 + p), \quad (4)$$

where a larger ratio gives straighter paths. Note that $(\sigma^r_1 - \sigma^r_2)$ is the magnitude of the remote differential stress, while the fracture driving stress, $(\sigma^r_1 + p)$, determines the strength of near-tip stresses (see equation 3a). The degree of path curvature in a developing fracture set is apparently determined by a competition between the remote stress state and the local fracture-induced stresses.

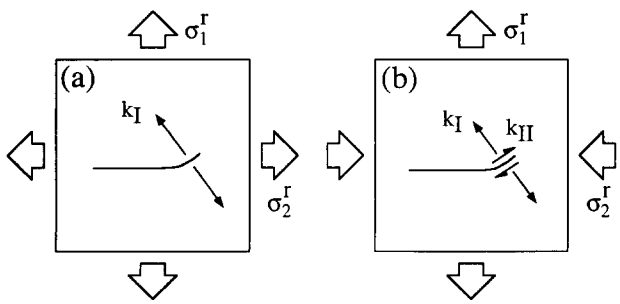

Fig. 2. A large remote differential stress, $\Delta\sigma^r = \sigma^r_1 - \sigma^r_2$, inhibits fracture curvature. (a) Isotropic remote stresses ($\Delta\sigma^r = 0$) resolve little to no shear across the tip of a curving fracture, while (b) a large $\Delta\sigma^r$ resolves into shear stress (k_{II}) and diminshed opening mode stress (k_I) across the curving fracture tip, thus pushing the fracture back toward a straight path.

EXPERIMENTAL WORK

While field examples of curving and straight overlapping fracture traces provide the motivation for this research, our notions of the mechanisms controlling fracture propagation paths can only be rigorously tested by measuring the geometry of fractures grown under well-known and reproducible conditions. Most field examples preserve only a small subset of the needed information, so we have turned to experimental methods. Here, we describe a set of experiments which investigate the two-dimensional propagation paths of echelon fractures in PMMA plates as a function of the applied biaxial loading and the initial geometry of a simple fracture array.

Methods

PMMA (polymethyl methacrylate) is a transparent plastic otherwise known as acrylic or by the brand names Perspex and Plexiglass. The deformation of polymeric materials is sensitive to temperature and strain rate (Cheng *et al.* 1990), but at room temperature, cast blocks or sheets of PMMA provide an approximately isotropic and homogeneous material exhibiting brittle failure. These properties have made it popular for use in model experiments (e.g. Erdogan & Sih 1963, Radon *et al.* 1977, Broberg 1987). Published data for the Young's modulus, Poisson's ratio and fracture toughness of PMMA at room temperature vary with loading rate, but $E = 3.10$ GPa, $\nu = 0.38$ and $k_{Ic} = 1.56$ MPa · m$^{1/2}$ are representative values (Hendry 1966, Radon *et al.* 1977). The machinability and transparency of PMMA simplifies the process of sample preparation and allows for visual inspection of fracture progress and surface texture.

In the experiments, two narrow, parallel starter slots (6.16 × 0.16 cm) are milled near the center of 4.5 mm-thick, cross-shaped sheets of PMMA (Fig. 3). The slot centers have a parallel *separation* of 19.0 cm and a perpendicular *spacing* of either 1.0, 3.0 or 6.0 cm. Small cracks 3±1 mm in length are notched into the inner tips of the starter slots by inserting and tapping on a knife blade. These cracks provide sharp fracture tips and insure that the slots will propagate toward the middle of the sample upon loading. The cruciform geometry provides a stress field across the center of the sample which is uniform to within ±7% (Fig. 4). The average stress in this working area is about 75% of the applied stress. The observed curvature in a crack path therefore may be largely attributed to mechanical interaction with the

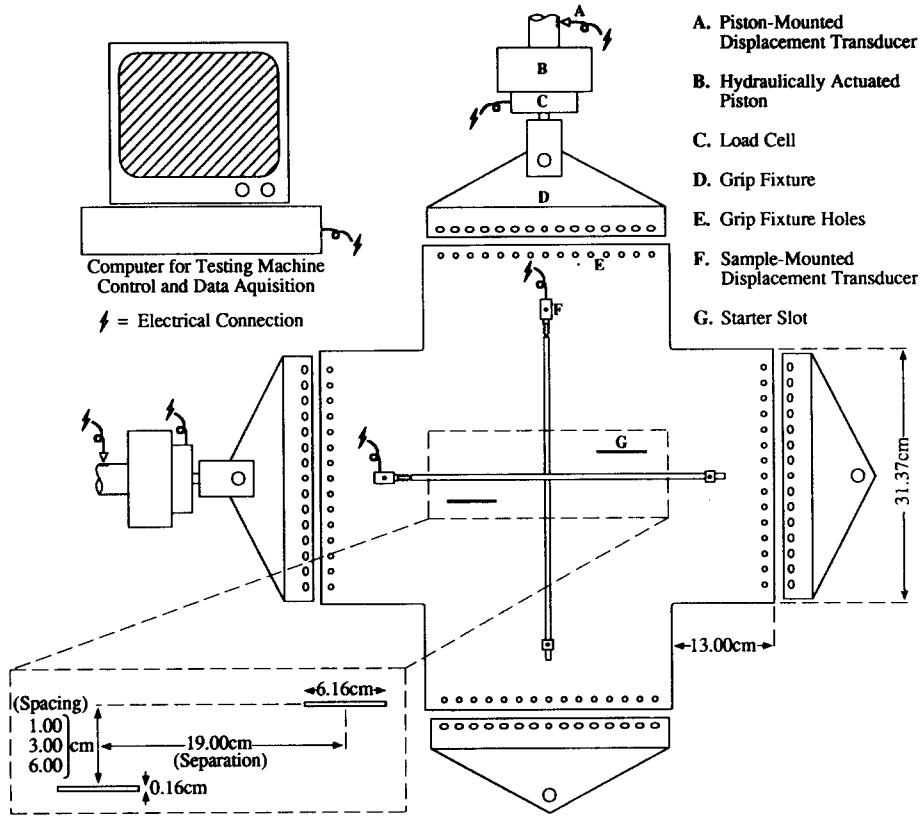

Fig. 3. Experimental method used to investigate fracture propagation paths in the laboratory. A 4.5 mm-thick, cross-shaped PMMA sheet is placed into a computer-controlled biaxial testing machine and attached to each of four hydraulically actuated pistons using grip-and-pin fixtures. Two starter slots are machined near the center of the sample and notched at their inner tips to insure that the fractures will propagate toward the center of the sample.

adjacent fracture, rather than to heterogeneities in the applied stress field.

The finished sample is placed into a computer-controlled biaxial testing machine and attached to each of four hydraulically actuated pistons using grip-and-pin fixtures (Fig. 3). The testing machine applies normal displacements to the sample according to a pre-defined loading program and automatically records force and displacement data from piston-mounted load cells and displacement transducers mounted both on the sample and on the pistons. Opposing pistons move inward or outward in harmony, so the specimen always remains centered in the machine. In the experiments described here, extension is gradually applied in a stepwise fashion perpendicular to the starter slots until one of the notched tips begins to propagate. As the fracture propagates across the sample, the applied displacements are gradually reduced or increased as necessary in order to control the speed of propagation. Because loading changes are required to limit the rate of fracture growth, we infer that propagation occurs near the dynamic limit (i.e. $k_I \geq k_{Ic}$). Propagation velocity is typically on the order of 1–10 mm s^{-1} and is always held well below the dynamic rate. The fracture is allowed to grow until it either intersects, overlaps and stabilizes, or bypasses the opposing starter slot. The fracture is considered *stabilized* when additional loading causes propagation from the unnotched end of the starter slot rather than continued forward growth.

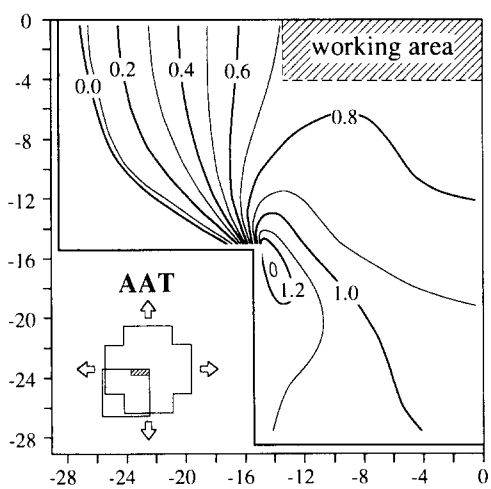

Fig. 4. The σ_{11} component of the stress field in one quadrant of a sample with no starter slots subject to all-around tension of unit magnitude. The stress field across the working area of the sample (where starter slots are machined) is uniform to within ±7% and averages about 75% of the applied load. Stresses were calculated using the boundary element method of Crouch & Starfield (1983). Scale is in centimeters.

Results

Three sets of experiments are presented for each fracture spacing. In each experiment (Fig. 5), every movement of the slot-perpendicular pistons is multiplied by a factor of either 1, 0 or −1 and applied to the slot-parallel axis, thus providing conditions of all-around tension (AAT), uniaxial loading (UNI) or crack-parallel

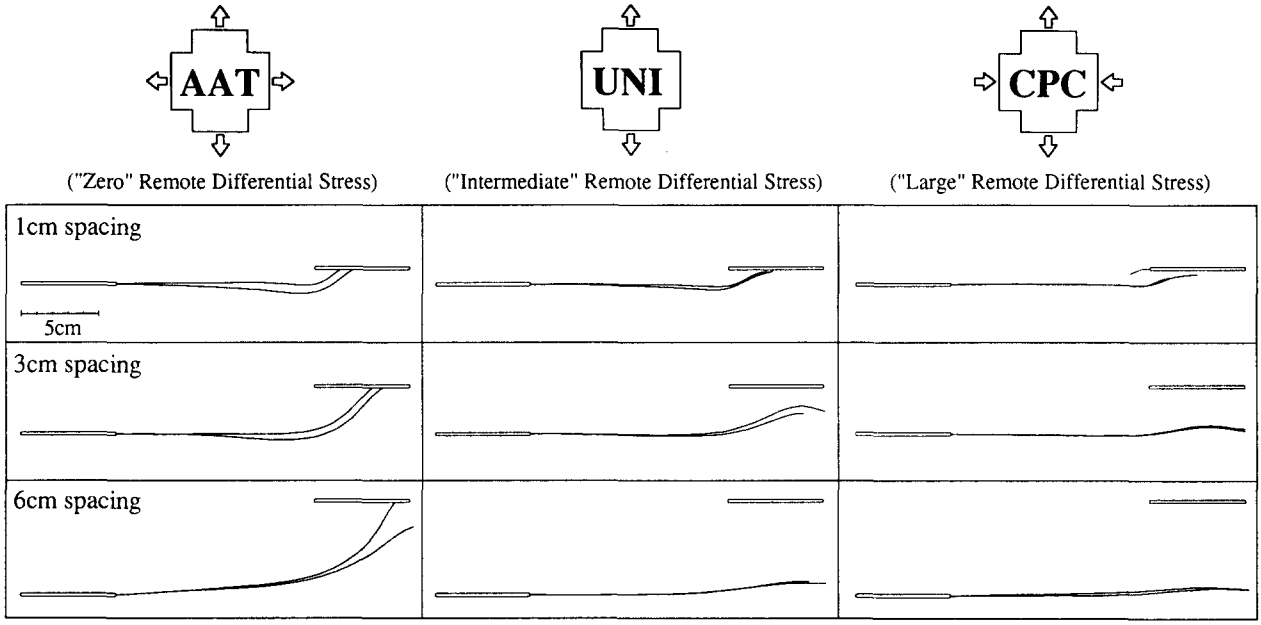

Fig. 5. Fracture paths generated in the laboratory. Two paths are shown for each loading-spacing combination, and the fractures are drawn as if they always initiated from the lower-left starter slot. The ratio of slot-parallel to slot-perpendicular applied displacements varies from 1 to 0 to −1, giving boundary conditions of all-around tension (AAT), uniaxial loading (UNI), and crack-parallel compression (CPC), respectively.

Table 1. Approximate stress boundary conditions provided by the AAT, UNI and CPC experiments. The open fractures are unpressurized free surfaces, so the fracture driving stress is given by $(\sigma_1^r + p) = \sigma_1^r$

Experiment	σ_2^r	$\Delta\sigma^r$	R
AAT	σ_1^r	0 ('Zero')	0
UNI	0	σ_1^r ('Intermediate')	1
CPC	$-\sigma_1^r$	$2\sigma_1^r$ ('Large')	2

compression (CPC). These boundary displacements approximate conditions of zero, intermediate and large remote differential stress at the center of the sample, giving remote stress-difference ratios of roughly 0, 1 and 2, respectively (Table 1). Two experiments were run for each loading and spacing combination, and the resulting paths are shown in Fig. 5.

Although every effort was made to machine similar starter slots and load them identically, in all cases a fracture propagated from only one of the two slots. Figure 5 is drawn as if the fracture always initiated from the lower-left starter slot, so that the paths can be overlain for direct comparison. In fact, initiation occurred from one or the other slot and the choice was not consistent. We attribute this to a greater stress intensity factor, k_I, at one of the notched tips due to slight disparities in loading, crack-tip sharpness and length. This demonstrates the sensitivity of fracture initiation to subtle and difficult to reproduce variations in loading and geometry. Despite the difficulty in predicting from which starter slot a fracture will grow, the ensuing propagation paths from repeated experiments are remarkably consistent.

The experimental results show that the paths of interacting echelon fractures are indeed sensitive to the remote differential stress, provided the fractures are not too closely spaced (Fig. 5). The 3 and 6 cm spacing experiments display paths which become progressively straighter as the remote differential stress is increased. The 1 cm spacing paths are far less responsive to changes in the remote stress state, and are instead dominated by the mechanical interaction between the fracture and slot. Regardless of the spacing, intersection was only achieved in the AAT experiments.

In one narrow spacing experiment, propagation began from the second slot as the first fracture tip approached (Fig. 5, CPC, 1 cm spacing). Subparallel fractures interact to increase k_I as they draw near and begin to overlap (Pollard *et al.* 1982, Cruikshank *et al.* 1991). At this narrow spacing, the added tensile stress induced by the approaching fracture was apparently sufficient to raise k_I to k_{Ic}. The two curving crack tips locally traced out similar paths even though their overall lengths differed by a factor of three. This supports the conclusion that the local stress fields arising from mechanical interaction were the controlling influence.

NUMERICAL WORK

Olson & Pollard (1989, 1991) modified the boundary element, displacement discontinuity method of Crouch & Starfield (1983) to model the growth of echelon joints and veins. In this two-dimensional, linear elastic, plane strain (or plane stress) boundary element method, the interior and exterior boundaries of a body are subdivided into N line segments across which there is a discontinuity in displacement with normal and shear components D_n and D_s (Fig. 6). A stress or displacement imposed across one element affects the stresses and displacements across all of the others, and in order to match the desired boundary conditions on each element, one must solve a linear system of $2N$ equations for $2N$

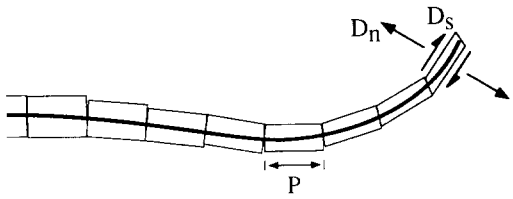

Fig. 6. In the boundary element numerical method of Olson & Pollard (1989), a fracture is divided into boundary elements of equal patch length, P, laid end-to-end. Each element is a line segment across which there is a discontinuity in displacement with normal and shear components D_n and D_s. Stress intensity factors, k_I and k_{II}, are calculated from the magnitudes of D_n and D_s across the crack-tip element. No special crack-tip element is used. Propagation is simulated by adding additional elements to the end of the fracture.

unknowns. The factor of 2 arises because there are two components of displacement or stress (traction) that determine the boundary conditions on an element. Using this method, a fracture of length L can be modeled by N elements of constant patch length, $P = L/N$, laid end-to-end. For a straight, uniformly loaded crack, Olson (1991) compared the D_n and D_s calculated for the crack tip element to the analytical solution for crack-wall opening and shearing (Pollard & Segall 1987) and arrived at the following expressions for k_I and k_{II}

$$k_I = 0.806 \frac{D_n E\sqrt{\pi}}{4(1-\nu^2)\sqrt{P}} \tag{5a}$$

$$k_{II} = 0.806 \frac{D_s E\sqrt{\pi}}{4(1-\nu^2)\sqrt{P}}. \tag{5b}$$

Equations (5a) and (5b) also were tested against the solution technique of Pollard & Holzhausen (1979) for the case of closely spaced, straight, echelon cracks. The margin of error was found to be less than 5% even when each crack was divided into only two elements (Olson 1991).

Computing k_I *and* k_{II} *for curved cracks*

The accuracy of equations (5a) and (5b) has previously been verified only for straight cracks. As we wish to model the growth of curved cracks, it is useful to compare the stress intensity factors computed for a circular arc crack (Fig. 7) with the analytical solution of Muskhelishvili (Muskhelishvili 1952, Cotterell & Rice 1980):

$$k_I = (\pi a)^{1/2}\left\{\left[\left(\frac{\sigma^r_{11}+\sigma^r_{22}}{2}\right) - \left(\frac{\sigma^r_{11}-\sigma^r_{22}}{2}\right) \times \sin^2(\alpha/2)\cos^2(\alpha/2)\right]\frac{\cos(\alpha/2)}{[1+\sin^2(\alpha/2)]} + \left(\frac{\sigma^r_{11}-\sigma^r_{22}}{2}\right)\cos(3\alpha/2) - \sigma^r_{12} \times [\sin(3\alpha/2) + \sin^3(\alpha/2)]\right\} \tag{6a}$$

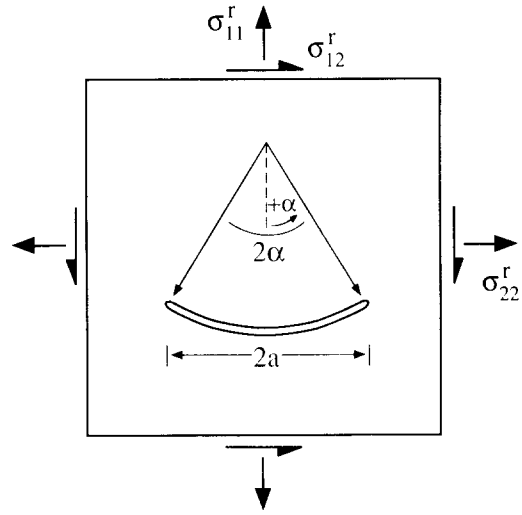

Fig. 7. The circular arc crack of Muskhelishvili (1952). The crack subtends an angle of 2α and has a projected width of $2a$.

$$k_{II} = (\pi a)^{1/2}\left\{\left[\left(\frac{\sigma^r_{11}+\sigma^r_{22}}{2}\right) - \left(\frac{\sigma^r_{11}-\sigma^r_{22}}{2}\right) \times \sin^2(\alpha/2)\cos^2(\alpha/2)\right]\frac{\sin(\alpha/2)}{[1+\sin^2(\alpha/2)]} + \left(\frac{\sigma^r_{11}-\sigma^r_{22}}{2}\right)\sin(3\alpha/2) + \sigma^r_{12} \times [\cos(3\alpha/2) + \cos(\alpha/2)\sin^2(\alpha/2)]\right\}. \tag{6b}$$

The stress intensity factors for a circular arc crack of width, $2a$ = 1 m, divided into four, 10 and 50 patches of equal length were computed using the boundary element method and equations (5a) and (5b) for arc angles, 2α, ranging from 0° (straight) to 180° (semi-circular). The normalized k_I and k_{II} calculated for pure biaxial ($\sigma^r_{11} = \sigma^r_{22} = \sigma$; $\sigma^r_{12} = 0$) and pure shear ($\sigma^r_{11} = \sigma^r_{22} = 0$; $\sigma^r_{12} = \tau$) loading of unit magnitude are plotted against the analytical solution in Fig. 8. For a circular arc crack divided into 50 elements, the normalized k_I and k_{II} are always within 0.021 and 0.017 of the exact solution, respectively. These results suggest that if an arcuate portion of a crack which subtends an angle of 2α degrees is divided into at least $\alpha/2$ segments, the boundary element method and equations (5a) and (5b) give normalized stress intensity factors with errors of less than a few hundredths.

A mixed mode I–II propagation criterion

Once k_I and k_{II} have been determined, a mixed mode fracture criterion is needed to determine whether and in what direction the crack will propagate. For their numerical method, Olson & Pollard (1989) chose the maximum circumferential stress criterion of Erdogan & Sih (1963). This criterion, which has been tested for PMMA (Erdogan & Sih 1963) and for rock (Ingraffea 1981), is based on two hypotheses: (1) the crack propagates radially from its tip; and (2) it starts in the plane perpendicular to the direction of greatest tension. The angle of incipient propagation, θ_o, is therefore equal to

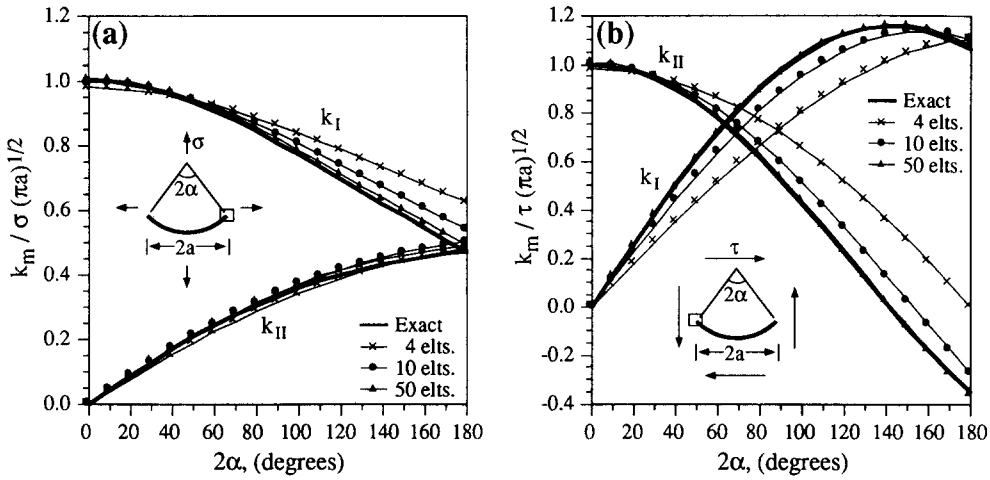

Fig. 8. Normalized k_I and k_{II} calculated for a circular arc crack of width, $2a$ = 1 m, subject to (a) pure biaxial ($\sigma^r_{11} = \sigma^r_{22} = \sigma$; $\sigma^r_{12} = 0$) and (b) pure shear ($\sigma^r_{11} = \sigma^r_{22} = 0$; $\sigma^r_{12} = \tau$) loading of unit magnitude using the boundary element method of Crouch & Starfield (1983) and equations (5a) and (5b). The analytical solution of Muskhelishvili (1952) is shown for comparison. The small boxes in the inset figures show for which crack tips k_I and k_{II} are plotted.

the angle, θ, which maximizes the tangential stress component, $\sigma_{\theta\theta}$, of the near-tip field (Fig. 1c). Differentiating equation (2b) and setting the result equal to zero yields

$$\cos\frac{\theta}{2}[k_I \sin\theta + k_{II}(3\cos\theta - 1)] = 0. \tag{7}$$

Which has the following solutions:

$$\theta = \pm\pi \tag{8a}$$

$$k_I \sin\theta_0 + k_{II}(3\cos\theta_o - 1) = 0. \tag{8b}$$

The solutions $\theta = \pm\pi$ correspond to the free surface condition, $\sigma_{\theta\theta} = 0$, at the crack walls, which is not of interest. Equation (8b) gives θ_o in terms of k_I and k_{II} (Erdogan & Sih 1963). A fracture subject to pure mode I loading ($k_{II} = 0$) propagates straight forward, $\theta_o = 0$, while pure mode II loading ($k_I = 0$) results in a kink angle of $\theta_o = -70.5°$ for $k_{II} > 0$ or $\theta_o = +70.5°$ for $k_{II} < 0$ (Fig. 9a). For computational purposes, it is useful to note that equation (8b) can be rewritten and solved directly for θ_o

$$\theta_0 = \sin^{-1}\left\{\frac{k_{II}}{k_I}\cos\phi\right\} - \phi \tag{9a}$$

$$\phi = \tan^{-1}\left(3\frac{k_{II}}{k_I}\right). \tag{9b}$$

Once the angle of incipient propagation has been determined, the maximum circumferential stress criterion calls on a third hypothesis: (3) propagation occurs when the distribution of tensile stress across the incipient plane of failure exceeds the fracture toughness, k_{Ic}, whose value is a property of the material

$$(2\pi r)^{1/2}\sigma_{\theta\theta}(\theta = \theta_o) = \cos\frac{\theta_o}{2} \times\left\{k_I\cos^2\frac{\theta_o}{2} - k_{II}\frac{3}{2}\sin\theta_o\right\} > k_{Ic}. \tag{10}$$

For pure mode I loading ($k_{II} = 0$), we have $\theta_o = 0$, and equation (10) reduces to the propagation criterion of classical fracture mechanics

$$k_I > k_{Ic}. \tag{11}$$

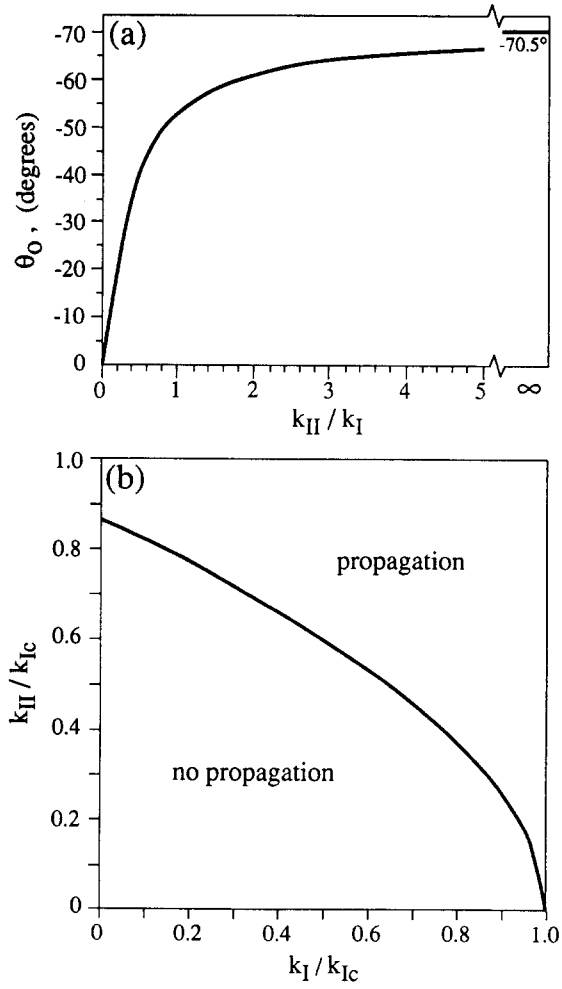

Fig. 9. Graphical representation of the maximum circumferential stress criterion (Erdogan & Sih 1963). (a) Angle of incipient propagation as a function of k_{II}/k_I. (b) The critical values of k_I and k_{II} required for opening mode propagation under mixed mode I–II loading.

A fracture subjected to mixed mode loading is therefore expected to propagate when

$$\cos\frac{\theta_o}{2}\left\{\frac{k_I}{k_{Ic}}\cos^2\frac{\theta_o}{2}-\frac{k_{II}}{k_{Ic}}\frac{3}{2}\sin\theta_o\right\}>1. \qquad (12)$$

The failure envelope predicted by equation (12) is shown in Fig. 9(b).

In geologic and engineering materials subjected to long-term loading, fracture propagation can be realized at values of k_I substantially lower than k_{Ic} (Atkinson & Meredith 1987). However, as long as the subcritical fracture follows a mode I path for which $k_{II} = 0$, the maximum circumferential stress criterion should still apply, provided we replace k_{Ic} in equation (12) with the threshold stress intensity factor for subcritical growth, k_{Io}.

Simulating the laboratory results

We now compare the predictions of the numerical method of Olson & Pollard (1989) to the fracture paths generated in the laboratory using PMMA. From a numerical standpoint, the initial problem is perfectly symmetric, but in order to match the laboratory results we allow propagation from only one of the two starter slots. The outer boundary of the sample is divided into 80 boundary elements either 2.60 or 3.14 cm in length, while each starter slot is divided into 20 boundary elements of equal length (3.08 mm). One additional element of the same patch length (3.08 mm) is added to the tip of the propagating slot at an angle of either 0° or ±10° to simulate the length and possible misalignment of the notched crack tip. Elements along the edges of the sample where grip fixtures attach are considered free of shear stress and are displaced inward or outward in a normal direction to simulate the loading applied by the testing machine. All other elements lie along free surfaces with zero normal and shear tractions. In the numerical calculations, an extension sufficient to initiate fracture is applied perpendicular to the starter slots and held constant as the fracture propagates. Slot-perpendicular displacements are multiplied by a factor of 1, 0 or −1 and applied simultaneously to the slot-parallel axis to simulate the AAT, UNI and CPC experiments, respectively.

Once the desired displacements on the boundaries of the cruciform sample have been applied, the boundary element method is used to solve for the stress field and the displacement discontinuity, D_n and D_s, across the crack-tip element. If the k_I and k_{II} calculated from equations (5a) and (5b) satisfy the failure criterion of equation (12), then a new element of the same patch length (3.08 mm) is added to the end of the crack at the angle, θ_o, given by equation (9). The added element perturbs the stress field, so the boundary element method is called upon after every iteration to recalculate the stress and displacement fields. This method inherently assumes quasi-static crack growth (i.e. well below the dynamic rate), so the applied displacements

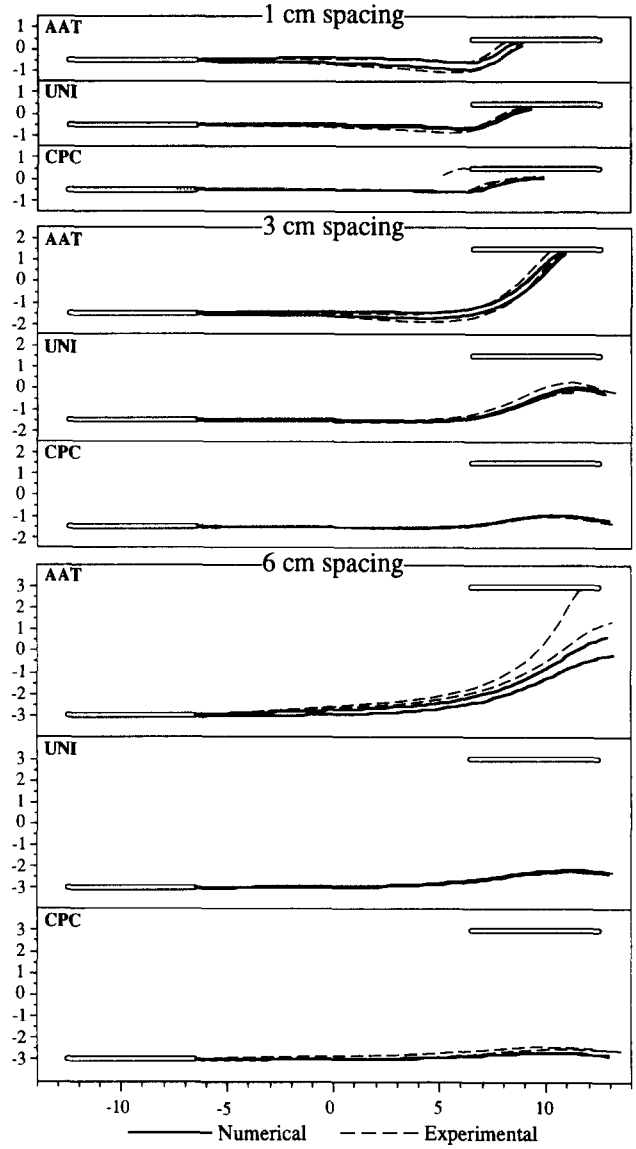

Fig. 10. Fracture paths predicted for the laboratory experiments using the boundary element numerical method of Olson & Pollard (1989) and a fracture patch length of 3.08 mm. The two paths shown for each loading and spacing combination correspond to initial misalignments of the notched crack with the starter slot of ±10°. Scale is in centimeters.

do not need to be varied in order to control the rate of propagation as was necessary for the laboratory experiments. The numerically calculated paths are plotted together with the experimental paths for comparison in Fig. 10, and their agreement is remarkable. The two numerical paths shown for each loading–spacing combination correspond to initial misalignments of the notched crack with the starter slot of ±10°.

NON-PERPENDICULAR INTERSECTIONS

An unexpected experimental result is the non-perpendicular intersection of fractures grown in the laboratory (Fig. 5, AAT experiments). Boundary conditions require that no shear stress can be resolved across the free surface of an open slot or fracture. In other words, this surface is a principal stress plane, and

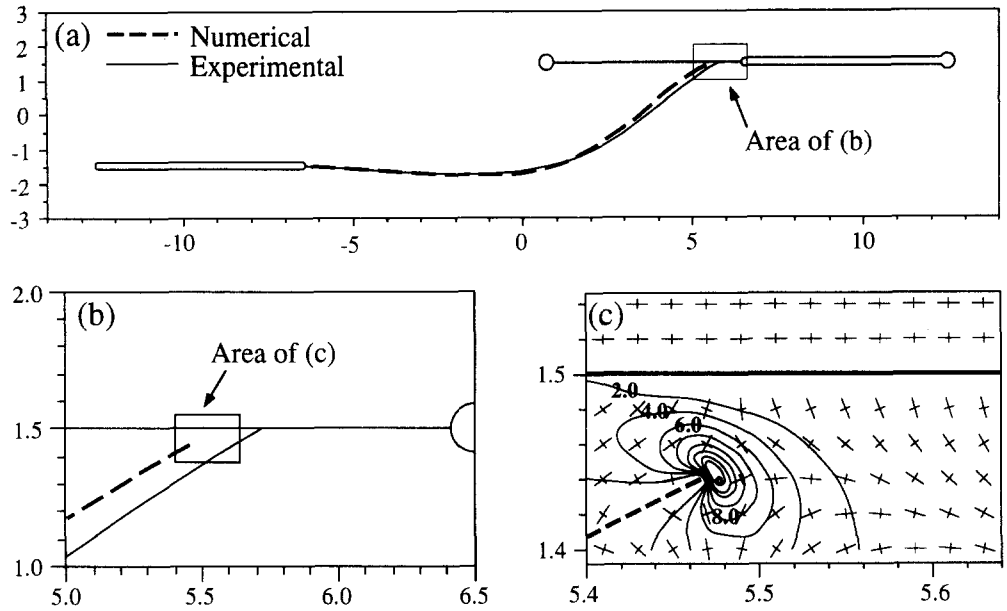

Fig. 11. (a) & (b) Numerical and experimental results suggest that a mode I fracture can intersect an adjacent, open fracture at an oblique angle, despite the free surface boundary condition at the crack wall. (c) A plot of the stress field just prior to intersection shows that stresses induced by the crack tip still dominate the local field. The contours and long tick marks give the magnitude (in MPa) and direction of the most tensile principal stress, σ_1, respectively. Scales are in centimeters.

the most tensile principal stress must lie either parallel or perpendicular to it, regardless of the remote field or the local fracture-induced field. If an approaching fracture follows a pure mode I path, we should expect it either to intersect the free surface at a right angle or to turn away and follow an asymptotic, non-intersecting path. The experimental paths which stabilize rather than intersect do follow asymptotic paths (Fig. 5, 1 cm UNI and CPC experiments), but even when viewed under a microscope, the approaches of intersecting fractures remain oblique.

From the laboratory results, it might appear that a non-mode I failure mechanism acts during the last increments of propagation. Additional experimental and numerical modeling, however, indicates that a mode I fracture can propagate very close to the free surface without turning perpendicular to it. Figure 11(a) shows a 3 cm spacing experiment in which the upper right starter slot was allowed to propagate a short distance under uniaxial loading. The sample was removed from the testing machine, and small holes were drilled at either end of the fractured slot to prevent further propagation. The sample was then placed back into the machine and subjected to AAT loading until a fracture propagated from the lower-left slot and intersected the adjacent crack. The intersection angle was oblique.

This laboratory experiment was simulated numerically by dividing the upper-right crack and lower-left slot into very small boundary elements with lengths of 0.75 and 0.50 mm, respectively. The numerical fracture path was then calculated to within 1.0 mm of intersection, giving an oblique approach almost identical to the experimental path. The results imply that the stresses generated at the tip of a propagating fracture so dominate the local field that the free surface condition has little effect on the mode I fracture path. A superimposed plot of stress trajectories and magnitude of the most tensile principal stress, σ_1 (Fig. 11c), provides additional evidence that this is the case. Note that even for this extremely small separation, the stress trajectories just ahead of the crack tip favor continued, straightforward propagation.

Of course, the numerical method preserves a simple linear elastic response to the very tip of the crack, whereas real materials have a zone of inelastic deformation about the tip (Kanninen & Popelar 1985, p. 146). For a propagating crack in PMMA, Lawn & Wilshaw (1975, p. 89) estimate an inelastic zone length of 0.8 mm. The mechanics of final intersection can only be modelled by explicitly including this zone. Nevertheless, the numerical model, which is valid so long as the distance between fractures exceeds the inelastic zone size, demonstrates that an opening mode fracture can propagate along an oblique path very close to the intersection with the free surface of another open fracture.

CRACK PATH STABILITY

Even in very homogeneous materials, a propagating fracture may encounter small-scale irregularities which cause it to deviate slightly from a mode I path. This problem is especially significant in rock, which can be very heterogeneous at the grain scale. For this reason, it is instructive to investigate the effect that a small kink at the crack tip has on the ensuing propagation path. For a straight crack subject to mixed mode loading, the stress intensity factors, K_I and K_{II}, at the tip of an infinitesimal kink may be expressed in terms of the stress intensity factors, k_I and k_{II}, at the tip of the main crack prior to kinking (Cotterell & Rice 1980, Melin 1987)

$$K_I = C_{11}k_I + C_{12}k_{II} \quad (13a)$$

$$K_{II} = C_{21}k_I + C_{22}k_{II}, \quad (13b)$$

where the C_{ij} are trigonometric functions of the kink angle, α (Fig. 12a). If the initial crack were subject only to pure mode I loading ($k_{II} = 0$), then to the first order

$$K_I = \tfrac{1}{4}[3\cos(\alpha/2) + \cos(3\alpha/2)]k_I \quad (14a)$$

$$K_{II} = \tfrac{1}{4}[\sin(\alpha/2) + \sin(3\alpha/2)]k_I. \quad (14b)$$

Cotterell & Rice (1980) show that equations (14a) and (14b) are accurate to within 5% for kink angles, α, as large as 90°. Because K_{II} at the tip of the kink is non-zero, the next increment of propagation will occur at some angle, θ_o, to the kink. Furthermore, because the sign of K_{II} and α are the same, θ_o and α have opposite signs, This insures that the kinked crack will at least initially turn back toward its previous path. In Fig. 12(b) we plot θ_o as a function of α using equations (9a) and (9b) and the ratio K_{II}/K determined from equations (14a) and (14b).

For our purposes, the infinitesimal kink is insignificant unless it leads to a significant departure of the crack from its previous path on the macroscopic scale. Therefore, the crack path can be considered stable when deviations arising from a small kink become negligible relative to the crack length as propagation continues (Melin 1983, Broberg 1987). For a straight crack parallel to x_2, subject to remote stresses $\sigma^r_{11} = \sigma^r_1$ and $\sigma^r_{22} = \sigma^r_2$, Melin (1983) uses a perturbation analysis to demonstrate that the crack path is stable so long as $(\sigma^r_1 - \sigma^r_2) > 0$. In other words, the propagation path of a straight crack is stable when the crack lies perpendicular to the most tensile (or least compressive) remote principal stress. If $(\sigma^r_1 - \sigma^r_2) < 0$, the crack diverges rapidly from its original plane after kinking. For isotropic remote stresses ($\sigma^r_1 = \sigma^r_2$), the crack path is indifferent, as the magnitude of deviation neither increases or decreases when normalized by the crack length (Broberg 1987, fig. 15). Fracture experiments in PMMA by Radon *et al.* (1977) confirm these expectations.

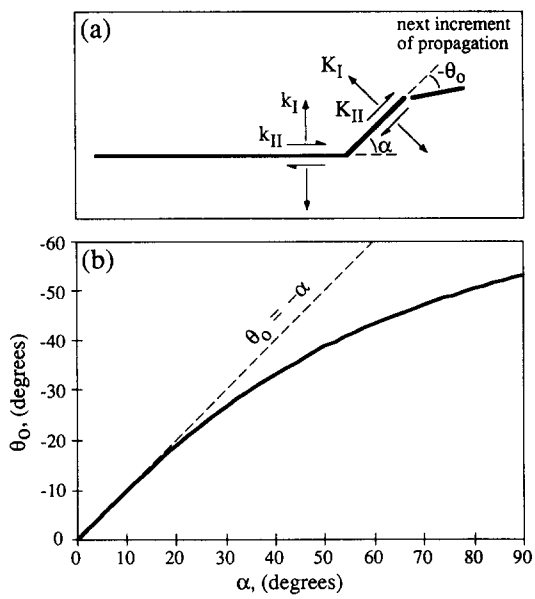

Fig. 12. (a) The stress intensity factors, K_I and K_{II}, at the tip of an infinitesimal kink of angle, α, can be written in terms of the stress intensity fractures, k_I and k_{II}, at the tip of the straight crack just prior to kinking. (b) If the unkinked fracture was subject to pure mode I loading ($k_{II} = 0$), then the angle of incipient propagation, θ_o, and α have opposite signs, and the fracture initially turns back toward its previous propagation path. Continued divergence or convergence from the previously straight path is governed by the orientation and relative magnitudes of the remote principal stresses.

Application to the experimental results

Inspection of Fig. 5 reveals that, while repeated UNI and CPC experiments produce consistently similar paths, the paths generated by AAT experiments are less reproducible. The numerically calculated paths (Fig. 10) also display this subtle variation. This observation is readily explained when we consider that the remote stress state approximated by AAT loading is essentially isotropic, so that small deviations from the ideal path (e.g. misaligned notches at the end of the starter slots) are not readily corrected by the influence of a remote differential stress during continued propagation. Small path disturbances in the UNI and CPC experiments, on the other hand, are rapidly damped out by a remote differential stress approximately equal to, and twice as great as, the fracture driving stress, respectively (Table 1).

Application to the numerical method

The fracture path length used to calculate the Fig. 10 paths was determined by dividing each starter slot into 20 boundary elements. Longer patches, however, produce paths which are similar to the Fig. 10 results, even when there are only a few elements per starter slot. Figure 13 shows the paths predicted for the 3 cm spacing experiments using a patch length of 20.53 mm, or just three elements per starter slot. Even though these elements are almost seven times longer than those used in Fig. 10 and are unable to capture the curving geometry

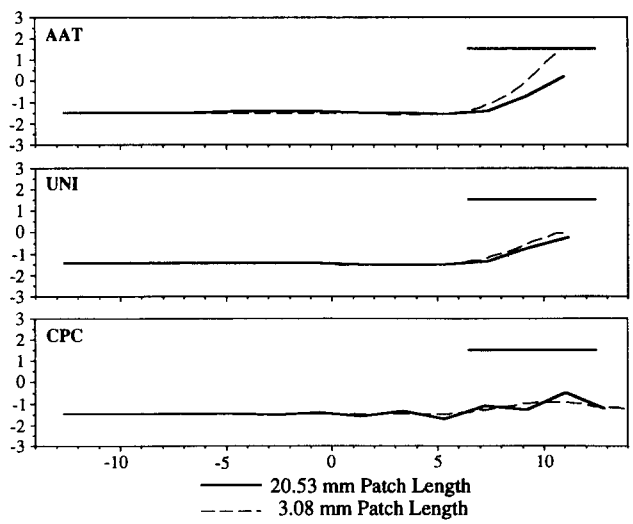

Fig. 13. A comparison of the numerical paths predicted for the 3 cm spacing experiments using a patch length of 20.53 mm with the paths predicted using much shorter 3.08 mm-long elements. Initial misalignment of the notched crack with the starter slot is assumed to be zero. Scale is in centimeters.

in detail, the predicted paths are quite similar. This rapid convergence occurs because a boundary element which is misaligned from the correct path will experience the same corrective mode II stresses as a misoriented fracture tip (Fig. 14). As with a curved or kinked crack, any errors in the calculated path are more strongly corrected by a larger remote differential stress.

Several mixed mode fracture theories besides the maximum circumferential stress criterion have been proposed to predict the onset and direction of propagation (Bergkvist & Guex 1979, Ingraffea 1981). Most are posed in terms of energy constraints, but all may be formulated in terms of the stress intensity factors k_I and k_{II}. When the ratio of k_{II} to k_I is large, the theories may differ significantly, yet in the limit as the loading becomes purely mode I ($k_{II} \rightarrow 0$), they converge to the common solution of $\theta_o = 0$ and $k_I > k_{Ic}$. Because a smoothly curving crack traces out a path for which $k_{II} = 0$, the resulting trajectory is largely independent of the choice among these criteria (Bergkvist & Geux 1979). Furthermore, a theory which incorrectly predicts the magnitude of the angle of incipient propagation can still produce accurate fracture paths provided it properly predicts the sign and the remote differential stress is non-zero.

This can be demonstrated readily by repeating the numerical simulation of the laboratory experiments while replacing equations (9a) and (9b) with a new, highly unrealistic equation for predicting the angle of incipient propagation

$$\theta_o = \begin{cases} -5°; k_{II} \geq 0 \\ 5°; k_{II} < 0 \end{cases}. \quad (15)$$

While this equation obeys the constraint that propagation angle is determined by the sense of shear, it completely ignores the magnitude dependence of θ_o on the ratio of mode II to mode I loading, k_{II}/k_I. During every increment of crack growth, the fracture propagation angle changes by +5° or −5°, so that even the path of a straight crack can at best be approximated by a sawtooth arrangement of elements. Nevertheless, the paths predicted using equation (15) are remarkably close to the original numerical results (Fig. 15), and only the AAT path, for which the remote differential stress is approximately zero, is significantly altered.

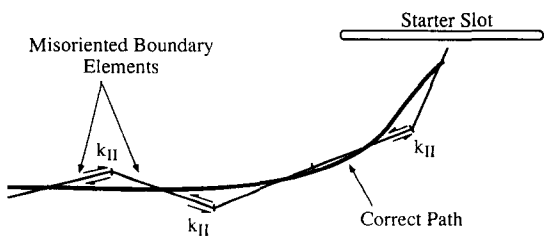

Fig. 14. Self-correcting nature of the numerical method used to calculate fracture paths. A misoriented boundary element at the fracture tip which strays away from the mode 1 path is subjected to mode II loading. The mode II stresses are always imposed with the proper sign (sense of shear) to bring the fracture tip back toward the correct path.

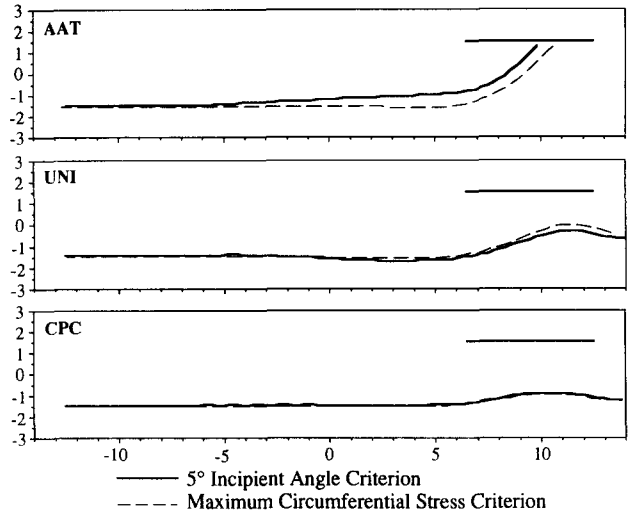

Fig. 15. A comparison of the numerically predicted paths for the 3 cm spacing experiments using the unrealistic 5° incipient angle criterion of equation (15) with the paths predicted using the maximum circumferential stress criterion. Except where the remote stress state is nearly isotropic (AAT loading), the constantly kinking 5° criterion path self-corrects and produces results that closely agree with the more sophisticated method. Initial misalignment of the notched crack with the starter slot is assumed to be zero. Scale in in centimeters.

Implications for rock fracture

The self-correcting nature of fracture paths under non-isotropic states of stress has important implications for rock fracture. The micromechanical mechanisms governing rock fracture can be quite complex, and over geologic time scales a fracture can propagate at stress intensities well below k_{Ic} (Atkinson & Meredith 1987). However, as long as the fracture attempts to follow a mode I path for which $k_{II} = 0$, the crack path predictions presented in this paper should still apply. A more serious concern is the heterogeneity of rock at the grain scale, but the results presented here indicate that the crack path should remain stable so long as the remote stress state is non-isotropic. Indeed, even a constantly kinking crack (Fig. 15) approximates the ideal path. Of course, rocks which have a strong fabric may behave anisotropically with respect to fracture strength and propagation at larger scales. These rocks would require different methods of analysis based on anisotropic materials.

CONCLUSIONS

The boundary element numerical method as adapted to opening mode fracture propagation by Olson & Pollard (1989) is successful in predicting experimental fracture paths in PMMA. Our laboratory results confirm the previous hypothesis (Olson & Pollard 1989, Cruikshank *et al.* 1991) that the relative straightness or curvature of echelon fracture traces depends on the fracture spacing and magnitude of the remote differential stress. Under non-isotropic states of stress, kinked or curved fracture paths are found to be self-correcting. Small-scale deviations of the fracture path at grain boundaries

in rock are therefore expected to be of little importance in determining large-scale fracture geometry. Our confidence is therefore enhanced that boundary element numerical methods can be used to produce and explain realistic fracture geometries in rock.

To our knowledge, the angular intersection of a fracture with an adjacent free surface has not previously been described. Additional experimental, numerical and theoretical work should help to determine what factors control the paths of intersecting fractures. Because the angle of intersection may provide another measure of the remote stress field, additional research on this subject would be worthwhile.

Acknowledgements—This research was supported by National Science Foundation (NSF) Grant EAR-8916676, by an Undergraduate Research Opportunities Grant from Stanford University, and by the Rock Fracture Project at Stanford University.

REFERENCES

Atkinson, B. K. & Meredith, P. G. 1987. The theory of subcritical crack growth with applications to minerals and rocks. In: *Fracture Mechanics of Rock* (edited by Atkinson, B. K.). Academic Press, London, 111–166.

Bergkvist, H. & Guex, L. 1979. Curved crack propagation. *Int. J. Fract.* **15**, 429–441.

Broberg, K. B. 1987. On crack paths. *Engng Fract. Mech.* **28**, 663–679.

Cheng, W.-M., Miller, G. A. Manson, J. A., Hertzberg, R. W. & Sperling, L. H. 1990. Mechanical behavior of poly(methyl methacrylate); part 1: tensile strength and fracture toughness. *J. Mater. Sci.* **25**, 1917–1923.

Cotterell, B. & Rice, J. R. 1980. Slightly curved or kinked cracks. *Int. J. Fract.* **16**, 155–169.

Crouch, S. L. & Starfield, A. M. 1983. *Boundary Element Methods in Solid Mechanics: With Applications in Rock Mechanics and Geological Engineering*. George Allen & Unwin, London.

Cruikshank, K. M., Zhao, G. & Johnson, A. M. 1991. Analysis of minor fractures associated with joints and faulted joints. *J. Struct. Geol.* **13**, 865–886.

Delaney, P. T. & Pollard, D. D. 1981. Deformation of host rocks and flow of magma during growth of minette dikes and breccia-bearing intrusions near Ship Rock, New Mexico. *Prof. Pap. U.S. geol. Surv.* **1202**.

Engelder, T. & Geiser, P. 1980. On the use of regional joint sets as trajectories of paleostress fields during the development of the Appalachian Plateau, New York. *J. geophys. Res.* **85**, 6319–6341.

Erdogan, F. & Sih, G. C. 1963. On the crack extension in plates under plane loading and transverse shear. *Trans. Am. Soc. Mech. Engng* **85**, 519–527.

Fleck, N. A. 1991. Brittle fracture due to an array of microcracks. *Proc. R. Soc. Lond.* **A432**, 55–76.

Hendry, A. W. 1966. *Photo-elastic Analysis*. Pergamon Press, Oxford.

Ingraffea, A. R. 1981. Mixed-mode fracture initiation in Indiana Limestone and Westerly Granite. In: *Proc. 22nd Symp. on Rock Mechanics*, 186–191.

Irwin, G. R. 1960. In: *Structural Mechanics: Proc. 1st Symp. Naval Structural Mechanics* (edited by J. N. Goodier & N. J. Hoff). Pergamon, Oxford, 557–591.

Kanninen, M. F. & Popelar, C. H. 1985. *Advanced Fracture Mechanics*. Oxford University Press, New York.

Lawn, B. R. & Wilshaw, T. R. 1975. *Fracture of Brittle Solids*. Cambridge University Press, Cambridge.

Melin, S. 1983. Why do cracks avoid each other? *Int. J. Fract.* **23**, 37–45.

Melin, S. 1986. When does a crack grow under mode II conditions? *Int. J. Fract.* **30**, 103–114.

Melin, S. 1987. Fracture from a straight crack subjected to mixed mode loading. *Int. J. Fract.* **32**, 257–263.

Muller, O. H. & Pollard, D. D. 1977. The stress state near Spanish Peaks, Colorado, determined from a dike pattern. *Pure & Appl. Geophys.* **115**, 69–86.

Muskhelishvili, N. I. 1952. *Some Basic Problems of the Mathematical Theory of Elasticity* (translated by Radok, J. R. M.). Nordhoff, Leyden.

Odé, H. 1957. Mechanical analysis of the dike pattern of the Spanish Peaks area, Colorado. *Bull. geol. Soc. Am.* **68**, 567–576.

Olson, J. E. 1991. Fracture mechanics analysis of joints and veins. Unpublished thesis, Stanford University.

Olson, J. E. & Pollard, D. D. 1989. Inferring paleostresses from natural fracture patterns: A new method. *Geology*, **17**, 345–348.

Olson, J. E. & Pollard, D. D. 1991. The initiation and growth of en échelon veins. *J. Struct. Geol.* **13**, 595–608.

Petit, J.-P. & Barquins, M. 1988. Can natural faults propagate under mode II conditions? *Tectonics* **7**, 1243–1256.

Pollard, D. D. & Muller, O. H. 1976. The effect of gradients in regional stress and magma pressure on the form of sheet intrusions in cross section. *J. geophys. Res.* **81**, 975–988.

Pollard, D. D. & Holzhausen, G. 1979. On the mechanical interaction between a fluid-filled fracture and the earth's surface. *Tectonophysics* **53**, 27–57.

Pollard, D. D. & Segall, P. 1987. Theoretical displacements and stresses near fractures in rock: with applications to faults, joints, veins, dikes, and solution surfaces. In: *Fracture Mechanics of Rock* (edited by Atkinson, B. K.). Academic Press, London, 277–349.

Pollard, D. D., Segall, P. & Delaney, P. 1982. Formation and interpretation of dilatant echelon cracks. *Bull. geol. Soc. Am.* **93**, 1291–1303.

Radon, J. C., Leevers, P. S. & Culver, L. E. 1977. Fracture toughness of PMMA under biaxial stress. In: *Fracture* 1977, *Vol.* 3. Waterloo, Canada, 1113–1118.

Ramsay, J. G. 1980. The crack–seal mechanism of rock deformation. *Nature* **284**, 135–139.

Segall, P. & Pollard, D. D. 1983. Joint formation in granitic rock of the Sierra Nevada. *Bull. geol. Soc. Am.* **93**, 1291–1303.

Sempere, J.-C. & Macdonald, K. C. 1986. Overlapping spreading centers: Implications from crack growth simulation by the displacement discontinuity method. *Tectonics* **5**, 151–163.

Shainin, V. E. 1950. Conjugate sets of en echelon tension fracture in the Athens limestone at Riverton, VA. *Bull. geol. Soc. Am.* **61**, 509–517.

Sumi, Y., Nemat-Nasser, S. & Keer, L. M. 1985. On crack path stability in a finite body. *Engng Fract. Mech.* **22**, 759–771.

Swain, M. V. & Hagan, J. T. 1978. Some observations of overlapping interacting cracks. *Engng Fract. Mech.* **10**, 299–304.